

Pulsed current electrodeposition of Ni/W-TiN coatings on X52 steel substrate. Surface characteristics and corrosion resistance

Lixin Wei¹, Yu Zhang^{1,}, Guifen Liu², Chunyang Ma³, Wei Zheng⁴*

¹ School of Petroleum Engineering, Northeast Petroleum University, Daqing 163318, China;

² Bidding Center, Jidong Oilfield Company, Tangshan 063004, China

³ College of Mechanical Science and Engineering, Northeast Petroleum University, Daqing 163318, China;

⁴ CNOOC Enter Tech-Drilling & Production Co. Shenzhen, Branch Guangdong, Shenzhen 518067, China

*E-mail: wangyiyouxiang1399@163.com

Received: 14 April 2021 / *Accepted:* 16 July 2021 / *Published:* 10 September 2021

The pulse current electrodeposition (PCE) technique was employed to successfully deposit Ni/W–TiN coatings on X52 steel. The effect of frequency and duty cycle on coating parameters like surface morphological characteristics, grain orientation, micro-hardness, crystal size, the number of deposited TiN CNPs, and corrosion resistance was investigated in detail. The findings show that TiN particles agglomerate, resulting in particle clouds with mean diameters of approximately 116.1 nm that are enclosed as second phases in the Ni/Co coating matrix. The Ni/W-TiN coating generated at a duty cycle of 10% and a pulse frequency of 10 Hz was able to process a maximum TiN content of 11.6 v/v%. It also showed that the coating grain became smaller when the duty cycle decreased or pulse frequency increased. The maximum micro-hardness value of the Ni/W-TiN coating synthesized at a duty cycle of 10% and a 10 Hz pulse frequency was 671.8 kg/mm, whereas the Ni/W-TiN coating deposited at 20 Hz and 30% had a maximum micro-hardness value of 642.4 kg/mm. Furthermore, the size of the semicircle was affected by charge-transfer resistance at the electrode/solution, therefore the size was observed to grow with the decrease in duty cycle and pulse frequency.

Keywords: oil pipeline; Ni/W–TiN coating; X52 steel; corrosion resistance; surface morphology

1. INTRODUCTION

Oil pipelines are well-known as the primary mode of remote oil transportation. X52 steel is a common material for oil pipelines. Corrosion in oil pipelines is a common occurrence owing to their

exposure to the climate, soil, water, and other environmental factors for a long time [1, 2]. As a result of its remarkable chemical, physical, and mechanical capabilities for safeguarding oil pipelines, the deposition of metallic matrix coatings has attracted the interest of researchers [3-6]. Metallic matrix coatings, including Ni/Mo-Al₂O₃ [7], Ni-SiC [8], Ni-TiN [9, 10], and Ni/Cu-WC [11], are composed of metal grains and ceramic nanoparticles (CNPs). The characteristics of Ni-based TiN composite coating on the metallic substrate include improved corrosion protection and tribological properties of X52 steels [12, 13]. Several investigations have shown that switching the matrix material from pure Ni to Ni or W-based alloys improves the main properties of Ni-based TiN [14-16]. The corrosion properties of the Ni/W-TiN based coatings have been widely studied [17-20], although there are few publications on the corrosion resistance characteristics of Ni/W-TiN coatings. The Ni/W-TiN coating is the metal-based TiN ceramic material prepared by using depositing TiN particles with Ni and W ions in the plating bath.

Pulse current electrodeposition (PCE) is a favorable, quick, and cheap processing technique for depositing Ni/W-TiN coating. Current density, frequency, duty cycle, plating bath composition, and other parameters, all have an impact on the net corrosion resistance of the coating [21-23]. In our previous research, we examined the impact of current density on nickel-based ceramic nanocoatings [24-26]. The goal of this study is to see if a Ni/W-TiN coating applied by PCE may improve mild steel corrosion resistance (MS). The effect of duty cycle and frequency on the coating parameters like crystal size, micro-hardness, surface morphology, grain orientation, the number of TiN CNPs deposited as well as its corrosion resistance was investigated and analyzed. The surface morphological characteristics of the coating were thoroughly investigated using scanning electron microscopy (SEM). The characterization of the coating's crystalline structural framework was carried out using X-ray diffraction (XRD), while the net amount of the deposited TiN nanoparticles was determined using the energy-dispersive X-ray spectrum (EDXS). In addition, the deposited coating was assessed for its micro-hardness and corrosion resistance.

2. EXPERIMENTAL SETUP

An electrode for electrodeposition was created using a sheet of X52 steel. An epoxy sealer was employed for sealing the specimen. A 2 cm² zone was left to be used as a working area. Before electrodeposition, the electrode based on steel was polished using 200, 800, and 1000 grit emery sheets, and then washed at room temperature with a 5 g/L NaOH + 20 g/L Na₂CO₃ solution before being activated for 20 seconds with a 1:1 HCl solution. A solution comprising NiCl₂•6H₂O 40 g/L, NiSO₄•7H₂O 250 g/L, WSO₄•7H₂O 70 g/L, TiN NPs (with a diameter of 40 nm) 10 g/L, boric acid 20 g/L and sodium citrate 25 g/L was placed within the plating bath and was used for the deposition of PCE. The aggregation of TiN NPs was prevented by the ultrasonic stirring of TiN NPs in the electrolyte before electrodeposition for 20 minutes at 200 W. In PCE deposition, X52 steel was connected to the negative of a DSM-100 pulse supply, whereas a nickel plate was connected to the positive of the pulse supply. The pulse frequency of the pulse supply varied between 1 and 20 Hz, and the duty cycles varied in the range of 10-70%. Table 1 enlists the variables for plating for PCE-deposition of surface coatings based on Ni/W-TiN.

Table 1. Plating parameters for PCE-depositing the Ni/W-TiN coatings.

Parameters	Values
Current density (A/dm ²)	4
Pulse frequency (Hz)	1, 10, 20
Duty cycle (%)	10, 30, 50, 70
pH	4.6
Bath temperature (°C)	50

The detailed morphological characteristics of the coating comprising Ni/W-TiN were studied using S3400 SEM, and the total amount of TiN NPs contained within the coating was estimated using EDXS in conjunction with SEM. The coating was kept at a thickness of 70 μm on average. For the determination of grain size and crystallographic orientation, an XRD assessment was carried out using an X-ray Diffractometer (Philips D5000) with a source providing Cu K α radiation. In this experiment, the scan rate was adjusted at 0.03 $^\circ$ /s, and the sample was scanned at two different angles ranging from 10 $^\circ$ to 80 $^\circ$.

The Ni/W-TiN coatings were examined for micro-hardness using a DT-950 Vickers Micro-Hardness Tester with a 100 g applied stress for 10s. For each sample, the mean value of a set of five measurements was acquired. For electrochemical impedance spectroscopy (EIS) calculations in simulated saltwater (seawater), MgCl₂ 2.5 g/L, MgSO₄ 3.3 g/L, aCaCl₂ 1.1 g/L, and NaCl 26.6 g/L were used to investigate the Ni/W-TiN coating in terms of their corrosion resistance. The EIS was measured using a CS350 electrochemical workstation equipped with a three-electrode cell. The standard calomel electrode (SCE) was employed as the reference electrode. The working electrode in the cell was 65 steel whereas a platinum sheet was used as the counter electrode. Before EIS analysis, the working electrode was immersed in seawater for 30 minutes till the attainment of consistent corrosion potential. The EIS was determined using a measurement frequency ranging from 10 mHz to 10 kHz and a 10-mV disturbance.

3. RESULTS

3.1. Structural analysis

Figure 1 illustrates the surface structural properties of the coatings based on Ni/W-TiN produced at several duty cycles and pulse frequencies of 10 Hz. The coatings have a needle-like and branching acicular morphology. As the duty cycle increases, the acicular structural frame transitions to a partly modular structure, with the acicular and spear-like trunks becoming shorter and closer to the branch length. In addition, as shown in Fig. 2, the coatings synthesized at 50% duty cycles are compared to those synthesized at 70% duty cycles in terms of surface morphologies; nevertheless, the coatings are

characterized at a rather low power of magnification than those in Fig. 1. The coatings synthesized at the lower duty cycle of 50% are stiffer and comparatively fine in structure in comparison to the ones synthesized at the high duty cycle of 70%.

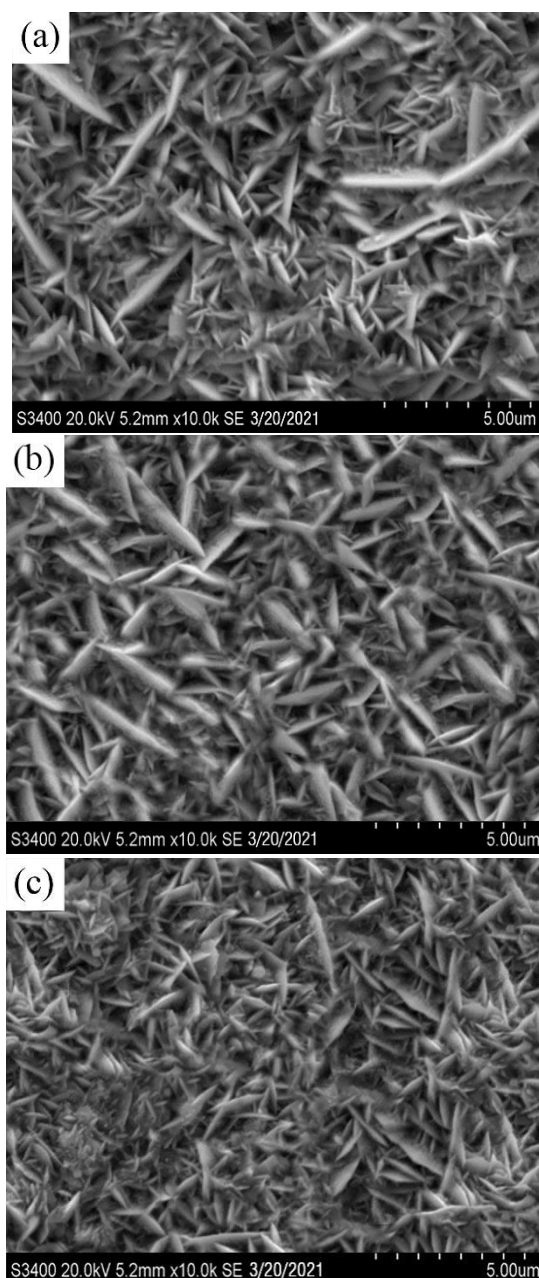


Figure 1. SEM photos of Ni/W–TiN coatings prepared at (a) 10%, (b) 50%, and (c) 70% duty cycles (Current density 4 A/dm², pulse frequency 10 Hz, pH 4.6).

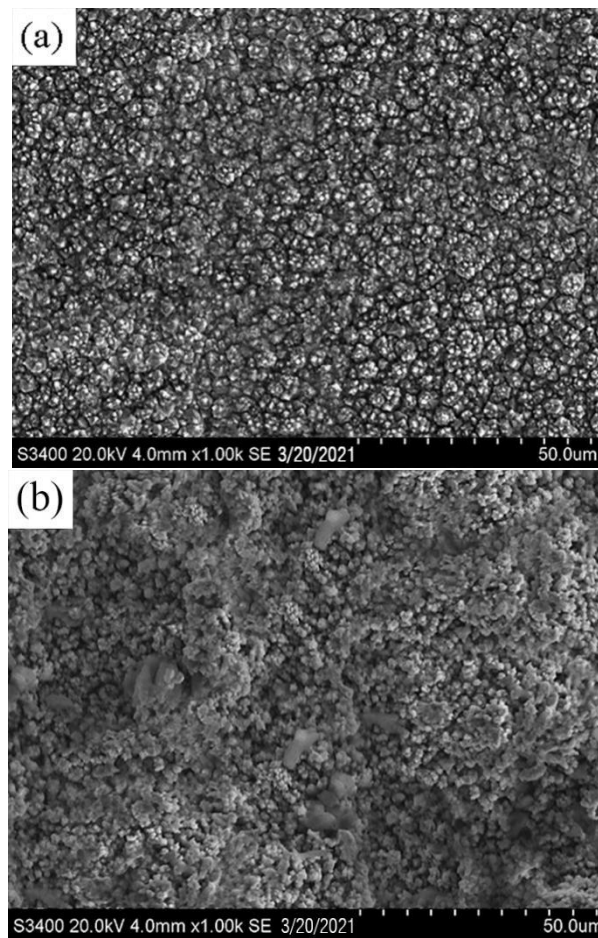


Figure 2. SEM photos of Ni/W–TiN coatings prepared at (a) 50% and (b) 70% duty cycles (Current density 4 A/dm², pulse frequency 10 Hz, pH 4.6).

Figure 3 outlines the surface morphological properties of the coatings comprising Ni/W–TiN synthesized at 30% duty cycle and varied frequency pulses. At 1 Hz, the covering has predominantly nodular morphology, with occasional short fibers here and there. The coating's morphology switches to acicular as the pulse frequency increases. When the frequency is increased to 10 Hz from 1 Hz, the total count and length of trucked fibers decrease, however, the branched fibers increase in number. Figure 4 depicts the surface properties of the TiN nanoparticles embedded within the layer. The TiN particles appear to agglomerate, resulting in clouds of particles with mean diameters around 116.3 nm that are enclosed as second phases within the matrix of a coating comprising Ni/W.

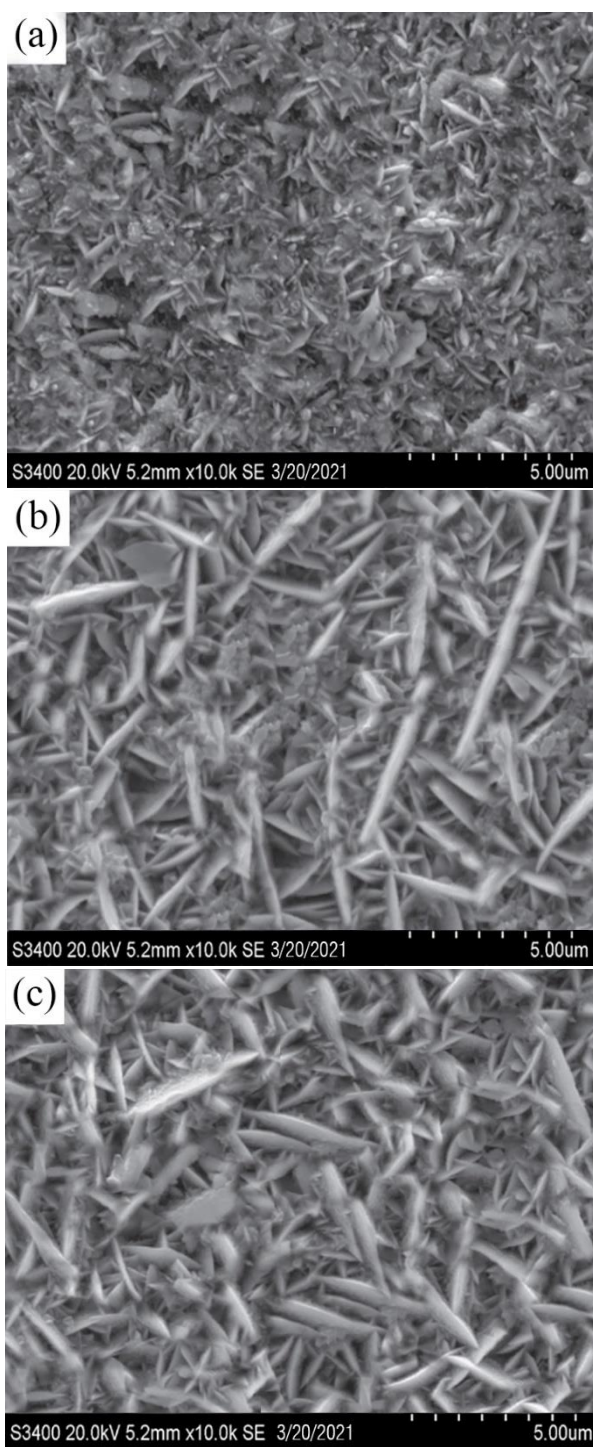


Figure 3. SEM photos of Ni/W-TiN coatings prepared at (a) 1 Hz, (b) 10 Hz, and (c) 20 Hz pulse frequencies (Current density 4 A/dm², duty cycle 30%, pH 4.6).

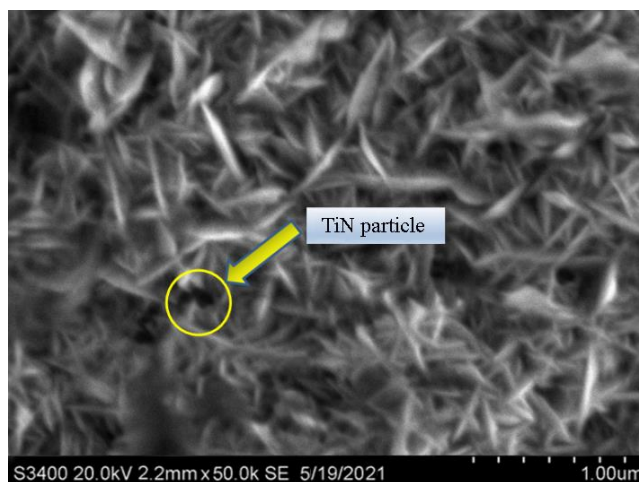


Figure 4. SEM photo of TiN nanoparticles (Current density 4 A/dm^2 , pulse frequency 10 Hz, duty cycle 30%, pH 4.6).

3.2. TiN content embedded within the coating

The percent volume of TiN nanoparticles implanted in the surface layer as a function of frequency and duty cycle respectively are depicted in Figures 5 and 6. As evident, the TiN concentration of Ni/W-TiN coatings undergoes an increment as the duty cycle is decreased and the pulse frequency is increased. Ni/W-TiN coating, which had a duty cycle of 10% and a pulse frequency of 10 Hz, was capable of processing a maximum TiN content of 11.6 v/v%. On the other hand, at 10 Hz and 70% duty cycle, the coating deposited had a minimum TiN content of 6.7 v/v%. Furthermore, the Ni/W-TiN coating placed at 1 Hz pulse frequency and a 30% duty cycle possessed the lowest TiN amount equivalent to 5.9 v/v%, whereas the Ni/W-TiN surface coating placed at 10 Hz and 30% contained the highest TiN content of 10.7 v/v%.

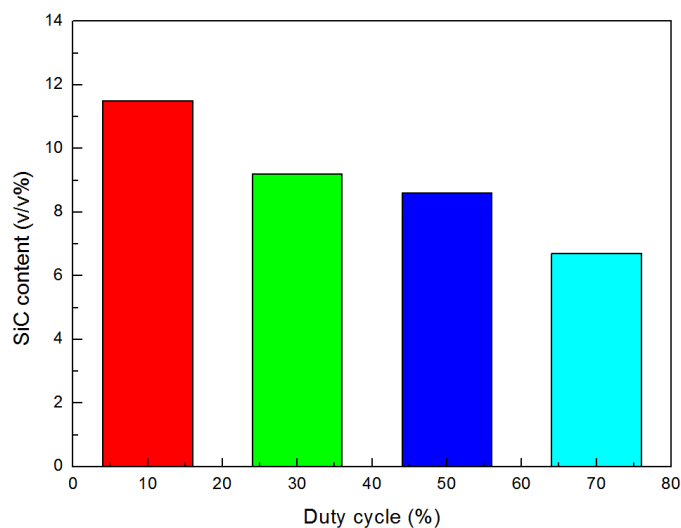


Figure 5. Influence of duty cycle on TiN contents in Ni/W-TiN coatings obtained at pulse frequency of 10 Hz (Current density 4 A/dm^2 , pH 4.6).

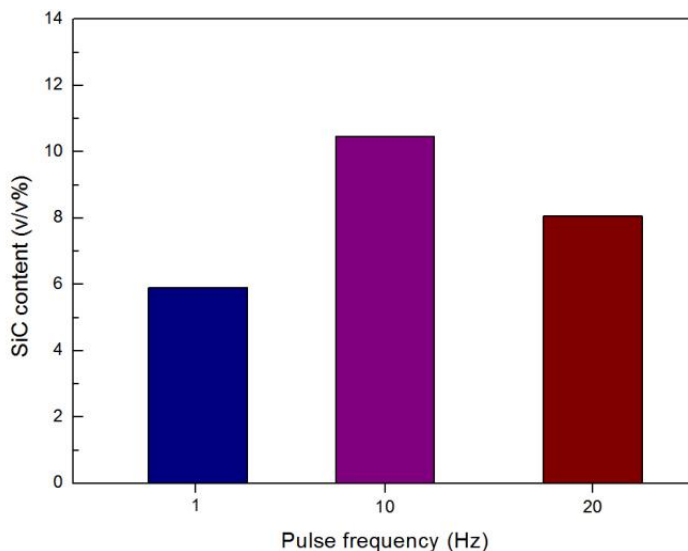
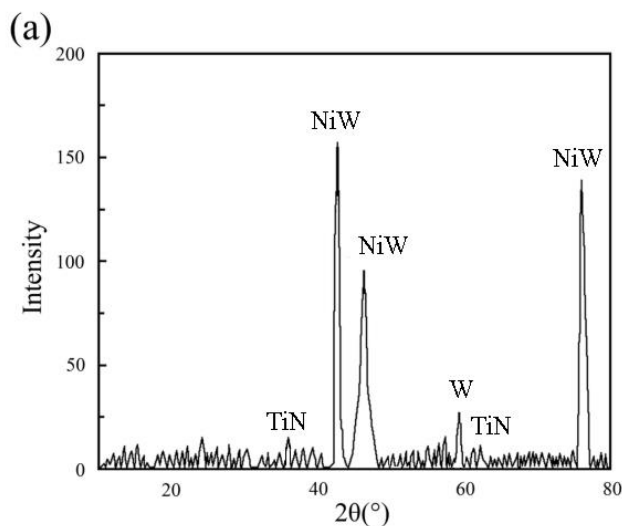


Figure 6. Influence of pulse frequency on TiN contents in Ni/W-TiN coatings obtained at duty cycle of 30% (Current density 4 A/dm², pH 4.6).

3.3. XRD characterization

Figures 7 and 8 depict the XRD spectrum of synthesized Ni/W-TiN coatings under the impact of various frequencies and duty cycles. Due to TiN, the weak characteristic line appears in the range of 2 Theta of 20~40° and 50~70°. TiN has an extremely low weight % because Ni and W have a density about three times that of TiN. As a result, the TiN peaks in the XRD data are somewhat weaker. Besides, owing to the existence of both W- and Ni-salts within the bath, NiW, and the other two phased-solid solutions are formed and recognized. Furthermore, when the frequency and duty cycle decrease, the typical inherent diffraction peaks belonging to the Ni/W-TiN coating become less intense. The XRD behavior of the deposited surface coating is not affected by changes in duty cycle and pulse frequency.



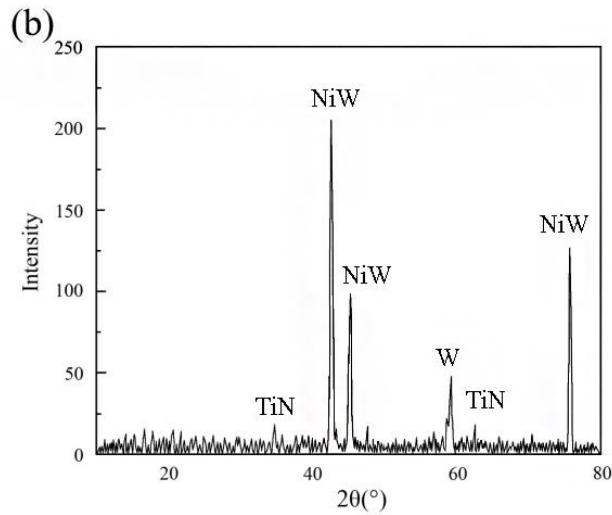


Figure 7. XRD spectra of Ni/W-TiN coatings obtained at (a) 10% and (b) 50% duty cycles (Current density 4 A/dm², pulse frequency 10 Hz, pH 4.6).

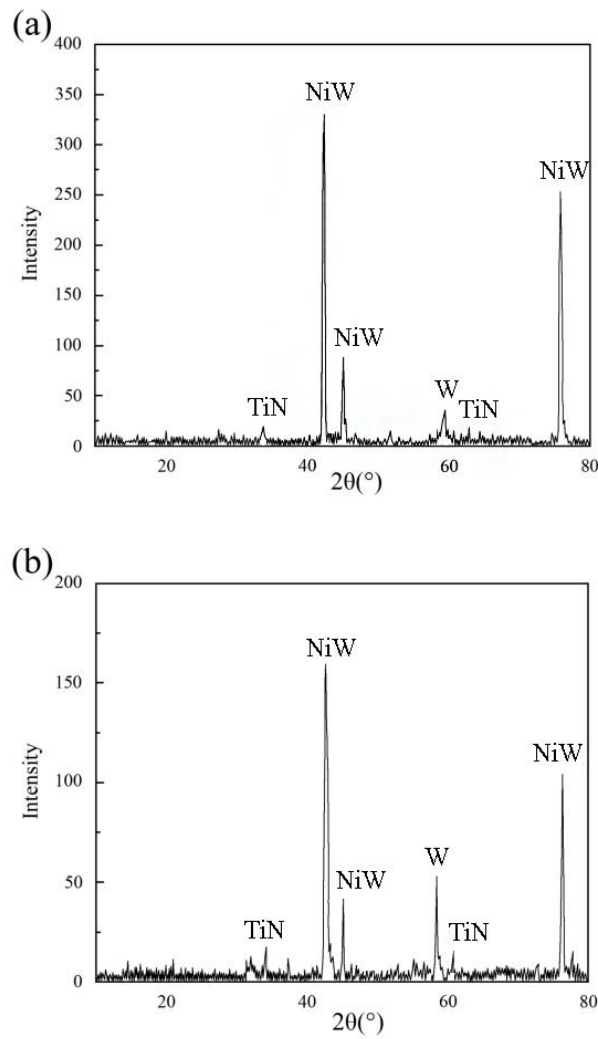


Figure 8. XRD spectra of Ni/W-TiN coatings obtained at (a) 1 Hz and (b) 10 Hz pulse frequencies (Current density 4 A/dm², duty cycle 30%, pH 4.6).

The XRD spectra are also used to estimate the dimensions of each grain within the composite, and Table 2 shows the relevant findings. It shows how the coating grain shrinks when the pulse frequency or duty cycle is increased. As a result, the grains in the coating are finer.

Table 2. Grain sizes in Ni/W-TiN composite deposited under different duty cycles and pulse frequencies (Current density 4 A/dm², pH 4.6).

Plating parameters		Average size (nm)
Duty cycle (%)	10	47
	30	52
	50	56
	70	61
Pulse frequency (Hz)	1	55
	10	51
	20	47

3.4. Micro-hardness test

The magnitudes of the micro-hardness for the coatings based on Ni/W-TiN with regard to differing duty cycles and pulse frequencies are shown in Figures 9 and 10. The coating's micro-hardness varies, as evidenced by the results, with values ranging from 510 kg/m to 680 kg/mm. The magnitudes of micro-hardness rise with the increase in frequency and reduction in the duty cycle. With a 10 Hz pulse frequency and a 10% duty cycle, the highest value of the micro-hardness of the synthesized Ni/W-TiN coating amounts to 671.8 kg/mm, whereas the Ni/W-TiN coating deposited at 30% and 20 Hz had a maximal magnitude of micro-hardness equivalent to 642.4 kg/mm.

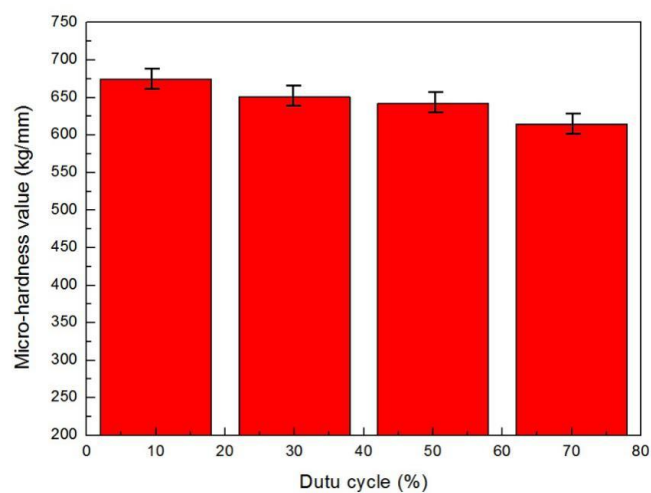


Figure 9. Column diagram of micro-hardnesses of Ni/W-TiN coatings obtained at 10 Hz (Current density 4 A/dm², pH 4.6).

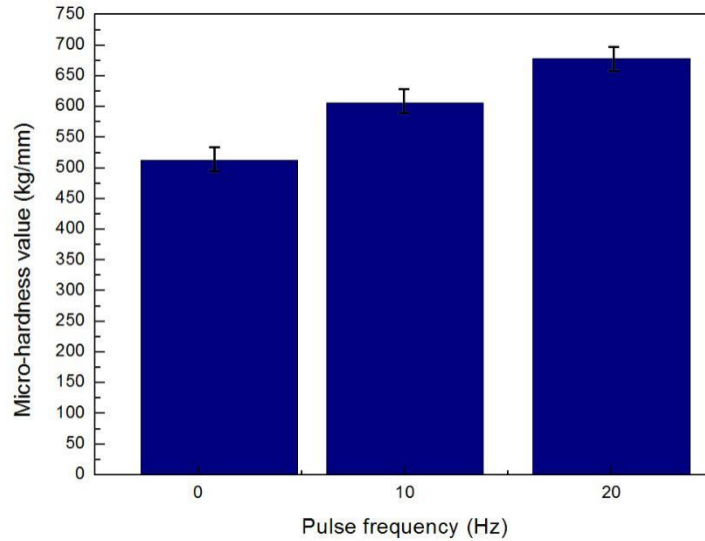
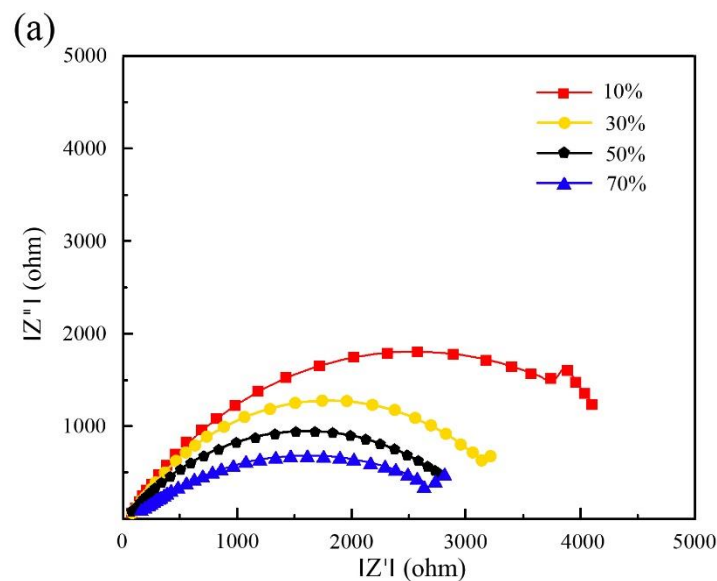


Figure 10. Column diagram of micro-hardnesses of Ni/W-TiN coatings obtained at 30% (Current density 4 A/dm², pH 4.6).

3.5. EIS Analysis

The estimated Nyquist and Bode graphs on the Ni/W-TiN coatings at different duty cycles and pulse frequencies are shown in Figures 11 and 12. A single semicircular form that spans the full frequency range is the feature of these curves. Nonetheless, the size grows as the pulse frequency and duty cycle drops since the size of the semicircle have been known to be influenced by the resistance offered at charge transfer at the electrode/solution.



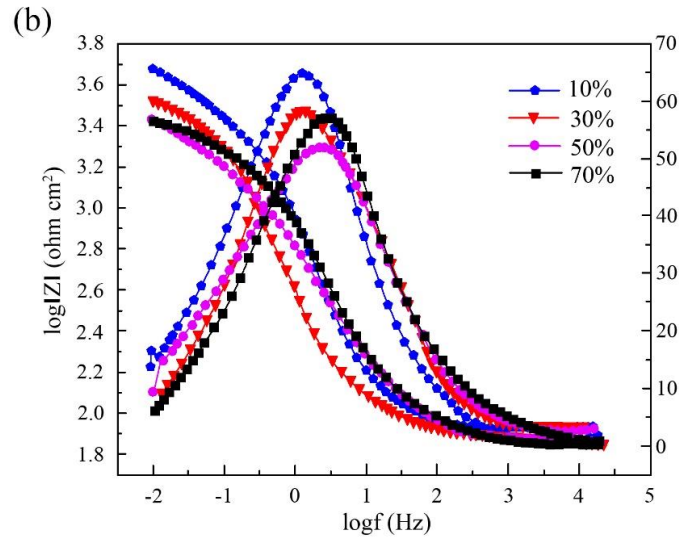


Figure 11. Nyquist (a) and Bode (b) curves of Ni/W-TiN coatings obtained at different duty cycles (Current density 4 A/dm², pulse frequency 10 Hz, pH 4.6).

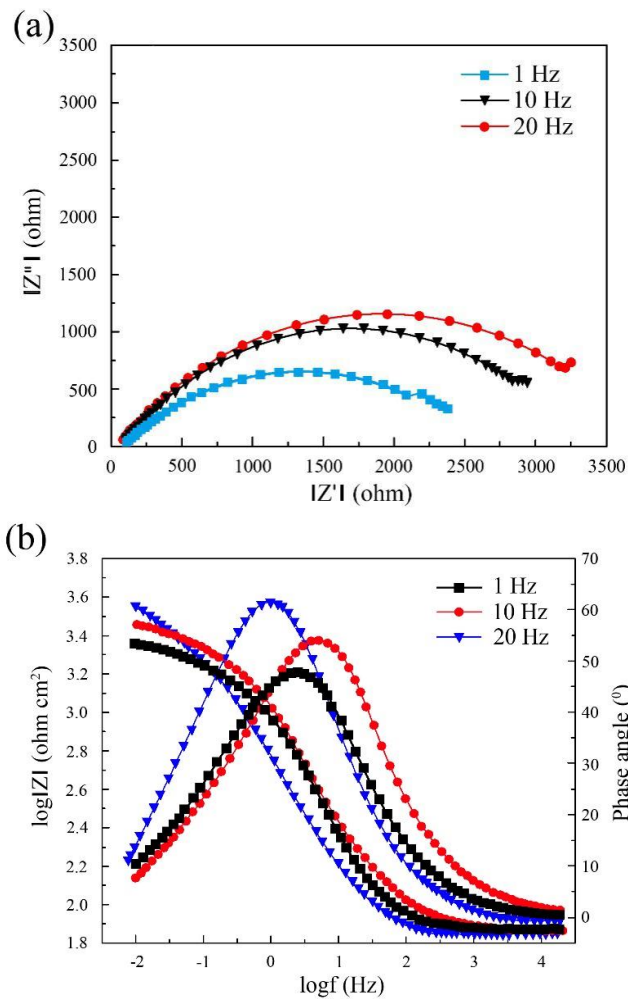


Figure 12. Nyquist (a) and Bode (b) curves of Ni/W-TiN coatings obtained at different pulse frequencies (Current density 4 A/dm², duty cycle 30%, pH 4.6).

4. DISCUSSION

4.1. Impact of plating parameters upon the deposition of TiN

The current study depicts that a reduced duty cycle allows for the deposition of a higher content of TiN particles. According to the two steps mechanistic details of adsorption proposed by Guglielmi, two sequential steps of adsorption lead to a total co-deposition of the un-reactive nanoparticles comprising TiN [27]. The first step entails loose adsorption of particles at the negative electrode, on the electrode itself, with a high extent of metal ion coverage, hence increasing the number of adsorbed particles to be deposited within the coating. Our findings also show that as the pulse frequency increases, the TiN content in the Ni/W- TiN coating increases at first, then declines marginally. A large overpotential can be generated during PCE deposition by using a correct pulse frequency (for instance 10 Hz), allowing more energy to be generated for adsorbing inert particles like TiN. The results are similar to those reported by Xia et al. [28].

4.2. Influence of plating parameters upon the microstructures of the coatings

Since the primary reflections of the solid solution based on Ni/W in the XRD spectrum occur from (1 0 0) and (1 1 0) planes, the prepared Ni/W-TiN coatings have a hexagonal close-packed (h c p) structure as shown in Figs. 7 and 8. Furthermore, with the reduction in the duty cycle and the increase in the pulse frequency, there is a shrinkage in the size of the grain, thereby influencing the net quantity of TiN particles embedded within the coated layer. Because the TiN particles serve as sites of nucleation for electrocrystallization, their existence has the potential to alter grain size, thus increasing the nucleation process while effectively retarding crystal growth. An impulse current having a high pulse frequency and low duty cycle, as previously discussed, might enhance the number of TiN grains deposited in the surface layer, thereby affecting the grain size in the process of electrodeposition.

Furthermore, the over-potential appears to be the variable used to determine the nucleation rate [29]. With a single pulse cycle, the high pulse frequencies could cause a large immediate over-potential, thereby increasing the rate of nucleation. This in turn slows down the grain's growth. Furthermore, a decrease in ON-time during one pulse cycle and a consequent decrement in the duty cycle might increase the charge-transfer current, which reduces grain development and increases nucleation rate.

4.3. Impact of plating parameters on mechanical characteristics and corrosion resistance of coatings

Generally, the hardness of TiN composite coatings based on Ni is affected by factors such as the number of hard particles inserted and the degree of hardness of the metallic matrix. The deposited nanoparticles inside a given metal matrix primarily influence the micro-hardness of a composite. The size and number of nanoparticles determine the mechanistic details of hardening, which are divided into two types. Particle strengthening and dispersion strengthening are the mechanisms involved [30]. Fine particles scattered within the matrix identify any materials that have hardened as a result of dispersion strengthening; the pinning of dislocations at particles that serve as dislocation pinning sites principally

determines the strengthening effect, which consequently leads to a rise in flow stress. While the matrix bears the load, the fine particles obstruct dislocation. On the contrary, a particle reinforced material is made up of big (>1 μm) particles along with a matrix. Despite the major load being taken by the matrix, a portion of it is carried by the particles as well, thereby preventing the deformation of the matrix.

In this work, dispersion strengthening is the major channel for increasing and boosting the coating micro-hardness since nanoparticles are used in electrode-deposition [31]. The particles in the composite contribute uniformly to the dispersion strengthening mechanism. The % count of particles in the composite increases as the particle size decreases, thereby improving the strengthening effect. Moreover, the grain size in the matrix influences the hardness of polycrystalline materials. The hardness of the composite normally increases as the grain size of the matrix is reduced. In this study, the microscopic shift in grain size caused by changing electrodeposition conditions was not enough to generate a significant difference in micro-hardness. The effects of pulse frequency and duty cycle on the micro-hardness properties of the surface layer are generally thought to be dependent on the number of deposited TiN nanoparticles.

To estimate the corrosion resistance of coatings synthesized by employing a multitude of electrodeposition conditions, we utilized an equivalent circuit model. This model consists of a charge-transfer resistance connected in parallel to a solution resistance, as well as a double-charge layer capacitance for the analysis of the electrochemical variables. As shown in Table 3, the charge transfer resistance varies with the pulse frequency and duty cycle and is inversely related to the rate of corrosion with respect to the pulse frequency and duty cycle. According to the findings, the charge-transfer resistance increases as the duty cycle undergoes a decrease, implying that the device has greater corrosion resistance. In addition, the charge-transfer resistance increases with the increase in the pulse frequency, thus manifesting an improvement in these composite materials in terms of their corrosion resistance.

Table 3. The charge-transfer resistance collected from EIS plots on Ni/W-TiN coatings (Current density 4 A/dm², pH 4.6).

Parameters		Charge-transfer resistance ($\Omega \text{ cm}^2$)
Duty cycle (%)	10	4911.5
	30	3664.7
	50	2925.3
	70	2796.2
Pulse frequency (Hz)	1	2657.1
	10	3122.4
	20	3478.9

It is possible to significantly improve the strength, hardness, structural well as chemical stability of the synthesized coatings by incorporating nanoparticles such as titanium dioxide (TiO₂). The improvement in these characteristics can potentially result in a greater level of corrosion resistance for

the coating. The presence of nonreactive TiN particles on the top layer also has the additional effect of decreasing the area that is effective for cathodic reduction. Consequently, anodic dissolution decreases as a result of this process. This phenomenon is consistent with the findings reported by previously published works [32, 33].

5. CONCLUSIONS

(1) An acicular and needle-like structure with a branched arrangement essentially characterizes the coatings. There is a gradual transformation of the acicular structural skeleton into a moderately nodular structural framework as the duty cycle increases, due to which the pointed and acicular trunks turn into shorter ones and become more closely aligned with the length of the branches. In addition, the TiN particles have a strong tendency to agglomerate, resulting in particle clouds with mean diameters of approximately 116.1 nm that are enclosed as second phases in the Ni/Co coating matrix.

(2) As maximum as 11.6 v/v% of TiN content was contained within the Ni/W-TiN coating synthesized at a 10 Hz pulse frequency and 10% duty cycle. On the contrary, the deposition of the coating at 70% duty cycle and 10 Hz yielded the coating with the lowest TiN quantity of 6.7 v/v%, which is significantly higher than the industry standard.

(3) Due to TiN, a weak characteristic line appears in the range of 2 between 20°40° and 50°70°. It also demonstrates that the coating grain becomes smaller with an increase in pulse frequency or a decline in duty cycle, as indicated by the graph.

(4) The Ni/W-TiN coating synthesized at a duty cycle of 10% and a pulse frequency of 10 Hz exhibited the maximum magnitude for micro-hardness at 671.8 kg/mm, while the Ni/W-TiN coating generated at a duty cycle of 30% and a pulse frequency of 20 Hz exhibited the maximum value of micro-hardness as 642.4 kg/mm.

ACKNOWLEDGEMENT

This work has been supported by the National Natural Science Foundation of China (Granted nos. 51974089), and Natural Science Foundation of Heilongjiang Province of China (Granted no. LC2018020).

References

1. Z. Wang and Z. Jian, *Corros. Rev.*, 34 (1-2) (2015) 17.
2. Y.P. Cheng, Z.L. Li, Y.L. Zhao, Y.Z. Xu, Q.Q. Liu, and Y. Bai, *Anti-corros. Method. M.*, 64 (4) (2017) 371.
3. F. Xia, Q. Li, C. Ma, W. Liu, and Z. Ma, *Ceram. Int.*, 46 (6) (2020) 7961.
4. F. Xia, Q. Li, C. Ma, and X. Guo, *Ceram. Int.*, 46 (2) (2020) 2500.
5. G. Bolelli, L.M. Berger, T. Boerner, H. Koivuluoto, L. Lusvarghi, C. Lyphout, N. Markocsan, V. Matikainen, P. Nylen, P. Sassatelli, R. Trache, and P. Vuoristo, *Surf. Coat. Technol.*, 256 (2015) 125.

6. S. Das, S. Banthia, A. Patra, S. Sengupta, and S.B. Singh, *J. Alloys. Compd.*, 738 (2018) 394.
7. F. Xia, Q. Li, C. Ma, D. Zhao, and Z. Ma, *Int. J. Electrochem. Sci.*, 15 (2020) 1813.
8. M. Alizadeh, and A. Cheshmpish, *Appl. Surf. Sci.*, 466 (2019) 433.
9. F.F. Xia, W.C. Jia, C.Y. Ma, R. Yang, Y. Wang, and M. Potts, *Appl. Surf. Sci.*, 434 (2018) 228.
10. X. Chen, and H.Y. Cheng, *Adv. Mat. Res.*, 912 (2014) 154.
11. J. Zhang, J. Lei, Z. Gu, F. Tantai, and Y. Fang, *Surf. Coat. Technol.*, 393 (2020) 125807.
12. W. Jiang, L. Shen, M. Qiu, X. Wang, M. Fan, and Z. Tian, *J. Alloys. Compd.*, 762 (2018) 115.
13. C. Ma, W. Yu, M. Jiang, and F. Xia, *Ceram. Int.*, 44 (5) (2018) 5163.
14. G. Prabhu, R. Arockia Kumar, and T.K. Nandy, *Int. J. Refract. Met. H.*, 82 (2019) 31.
15. A. Karimzadeh, M. Aliofkhazraei, and F.C. Walsh, *Surf. Coat. Technol.*, 372 (2019) 463.
16. Y. Liu, H. Lu, and X. Kou, *Int. J. Hydrog. Energy.*, 44 (16) (2019) 8099.
17. C. Ma, D. Zhao, and Z. Ma, *Ceram. Int.*, 44 (5) (2018) 5163.
18. P.Q. Dai, Y.H. Zhong, and X. Zhou, *Surf. Eng.*, 27 (1) (2011) 71.
19. G. Sharma, R.K. Yadava, and V.K. Sharma, *B. Mater. Sci.*, 29 (5) (2006) 491.
20. B. Bahadormanesh and A. Dolati, *J. Alloys Compd.*, 504 (2) (2010) 514.
21. Q. Fan, Y. Gao, Y. Zhao, Q. Yang, L. Guo, and L. Jiang, *Mater. Lett.*, 215 (2018) 242.
22. R. Sen, S. Das, and K. Das, *J. Nanosci. Nanotechnol.*, 10 (12) (2010) 8217.
23. M. Alizadeh and A. Cheshmpish, *Appl. Surf. Sci.*, 466 (2019) 433.
24. C. Ma, D. Zhao, H. Xia, F. Xia, Z. Ma, and T. Williams, *Int. J. Electrochem. Sci.* 15 (2020) 4015.
25. T. Liu, C. Ma, Q. Li, J. Li, F. Xia, and C. Li, *Int. J. Electrochem. Sci.*, 15 (2020) 12103.
26. F. Xia, C. Li, C. Ma, Qiang Li, and H. Xing, *Appl. Surf. Sci.*, 538 (2021) 148139.
27. N. Guglielmi, *J. Electrochem. Soc.* 119 (1972) 1009.
28. F. Xia, W. Yue, J. Wang, C. Liu, F. Wang, and Y. Li, *Ceram. Int.*, 41 (9) (2015) 11445.
29. C. Sun, X. Liu, C. Zhou, C. Wang, and H. Cao, *Ceram. Int.*, 45 (1) (2019) 1348.
30. G. Sharma, R.K. Yadava, and V.K. Sharma, *Bull. Mater. Sci.* 5 (2006) 491.
31. S. Dehgahi, R. Amini, and M. Alizadeh, *J. Alloys Compd.* 692 (2017) 622.
32. C. Ma, X. Guo, J. Leang, and F. Xia, *Ceram. Int.*, 42(8) (2016) 10428.
33. F. Xia, C. Liu, F. Wang, M.H. Wu, J.D. Wang, H.L. Fu, and J.X. Wang, *J. Alloy. Comp.*, 490 (2010) 431.